Available online at www.sciencedirect.com
ScienceDirect
Journal of Hazardous Materials 158 (2008) 438–444
Journal of Hazardous Materials
www.elsevier.com/locate/jhazmat

Air distribution and size changes in the remediated zone after air sparging for soil particle movement

Yih-Jin Tsai *

Department of Environment and Resources Engineering, Diwan University, No. 87-1, Nansh Li, Madou, Tainan, Taiwan

Received 13 November 2007; received in revised form 17 January 2008; accepted 26 January 2008
Available online 6 February 2008

Abstract

In an unconsolidated porous medium, soil particles can be mobilized by physical perturbation. In model systems of fluids flowing over spherical particles attached to flat surfaces, the hydrodynamic shear force depends on the fluid viscosity, particle radius, and flow velocity. Soil particles can be reasonably expected to be transported by flowing water during air sparging when the particle-size distribution does not fit the densest possible particle arrangement. If soil particles are transported during air sparging, then the distribution of the porosity and reservoir permeability will change. The remediated zone changes because of the changes in soil characteristics. This study applied some mathematical models to elucidate the mobilization process of soil particles during in situ air sparging. The changes in the characteristics of the soil and the swept volume of injected air during air sparging were also investigated. The results demonstrated that particle movement reduced the radius of influence (ROI) and the swept volume of injected air. In this case study, the maximum reducing rates in ROI and the swept volume were 24% and 26% for the zone where the gas saturation exceeded 10%.

Keywords: Air sparging; Particle movement; Internal stability; Swept volume; Radius of influence

1. Introduction

Air sparging below the water table, via a sparging well with a slotted screen removes volatile organic contaminants from the saturated zone. The efficiency of field remediation depends strongly on the flow path of the injected air, which in turn depends on the soil characteristics.

Braida and Ong [1] devised an experimental apparatus for monitoring the air flow path and measuring the mass transfer of volatile organic compounds (VOCs) during air sparging, and the results demonstrated that the size of the mass transfer zone was influenced by mean particle size and soil uniformity coefficient.

Ji et al. [2] performed laboratory flow visualization experiments and suggested that air channel formation was sensitive to the heterogeneities of soil matrix. McCray and Falta [3,4] devised the multiphase numerical simulation to measure the radius of influence (ROI) of sparging, and found that remediation effectiveness of air sparging varies significantly owing to heterogeneities and anisotropies in the porous medium. Reddy and Adams [5] performed a laboratory test, using air sparging, to examine the effect of soil heterogeneity on the removal of benzene. The results showed that the injected air followed the path of least resistance and avoided regions with low permeability. These results indicate that the heterogeneity of soil matrix seriously affects the air flow path.

Santarelli et al. [6] presented a field case study of oil reservoir in the Norwegian Sea where the phenomenon of sanding was observed. Papamichos et al. [7] developed a model that estimates the volume of sand production from a hollow cylinder test on a weak sandstone. The results demonstrated that the rate of sand production increased with external stress and fluid flow rate. Moghadasi et al. [8] presented the results of an experimental and theoretical study on the mechanisms of formation damage caused by invasion of solid particles and their deposition into a porous medium. Changing in permeability was observed in their cases. Sanding is assumed to have been caused by the rock around the producing well, which is too weak to sustain the shear stresses.

In an unconsolidated porous medium, soil particles of the aquifer are mobilized by physical perturbation. O'Neill [9]

* Tel.: +886 6 5718888x871; fax: +886 6 5718014.
E-mail address: yjtsai@mail.dwu.edu.tw.

0304-3894/$ – see front matter © 2008 Elsevier B.V. All rights reserved.
doi:10.1016/j.jhazmat.2008.01.089

developed model systems of fluids flowing over spherical particles attached to flat surfaces. The hydrodynamic shear force F_{shear} of the system depended on the fluid viscosity μ, particle radius r, and flow velocity U_r:

$$F_{shear} = 1.7009(6\pi)\mu r U_r \quad (1)$$

Eq. (1) reveals that the shear force increases with increasing velocity U_r. The particle is mobilized if the hydrodynamic shear force exceeds the gravity and resistance. Sanding of well is one of the common problems during groundwater pumping of aquifers, especially in fine sand or silty formations [10]. For this reason, many groundwater wells use the conventional design consisting of a slotted screen with a bottom sump that provides the filter and the place for fine solids to settle as they are drawn into the well. In the field of soil mechanics, soil scientists have focused on particles mobilized by the infiltration of rainwater. Zevi et al. [11] studied the particle behavior by quantifying particle movement and retention as observed in pore-scale image sequences. Kaplan et al. [12] reported that the amount of particles mobilized is directly related to the flow rate of free-flowing soil water. The size of the mobilized particles increases with the rate of infiltration. Kaplan et al. [13] demonstrated that particle concentrations eluted from repacked lysimeters are directly related to the kinetic energy of moving water. In air sparging, the velocity of flowing air or flowing water is 10–100 times greater than that due to rainwater infiltration. Soil particles can be reasonably expected to be transported by flowing air and water during air sparging. Reddi and Govindaraju [14] studied the transport of contaminants associated with fine particles in porous media in the context of groundwater remediation. Their experimental results indicate that the rate of application of pressure gradient is a significant factor in controlling the detachment of fines. Tsai and Lin [15] monitored soil particle movement by performing a sandbox test and showed that the change in soil porosity is directly proportional to the flow rate. Tsai [16] performed a tracer test to monitor the air flow path and studied the soil particle movement during in situ air sparging.

The foregoing studies demonstrate that soil particles can be transported by flowing water during air sparging. This phenomenon changes the sort of soil matrix, permeability and the distribution of porosity. Such changes may probably change the flow path of the injected air.

The objective of this work is to use simple mathematical models to assess the change in air distribution caused by a single air injection well in an unconsolidated aquifer. The study focuses not on mass removal rates or mechanisms, but rather on assessing the change in the air distribution and the size of the remediated zone in cases where the soil particles were transported during air sparging.

2. Model and theory

2.1. Basic assumptions and hydro-mechanical equations

The proposed model simulates the flow of soil particles during air sparging, consequent changes in porosity and permeability, and the resultant changes in air flow. Soil particle stability is critical to particle movement in this study.

2.1.1. Internal stability of particle

The term "internal stability" describes the ability of granular material to prevent loss of its own small particles because of disturbances such as fluid flow. A material that does not lose particles is considered to have a stable gradation, and one that loses particles to have an unstable gradation.

Particle size and size distribution are the most important determinants of soil stability during air sparging. If the particle-size distribution allows the densest possible particle arrangement, or if the fine particles exactly fit the voids formed by coarser particles, then the soil particles cannot be lost. Not all sand particles in the soil are transportable by water. Only those sand particles that are smaller than the pore size are transportable. Some assumptions are necessary to simplify the complex multiphase flow and soil structure.

(1) The transporting ability of water significantly exceeds that of air. The soil particles just move with the water.
(2) The saturated porous medium is modeled as a three-phase system consisting of skeleton solids, fluidized-solids and fluid.
(3) Fluidized particles are particles in suspension that move with the fluid. The other loose particles, which are trapped inside the void space, are considered part of the solid phase.
(4) The solid is assumed to be rigid. That is, a solid particle either has zero velocity and is assigned to the solid phase, or has the velocity of the fluid and is assigned to the mixture, which fills the void space. The volume fraction of voids is expressed by bulk porosity ϕ thus

$$\phi = \frac{dV_v}{dV} \quad (2)$$

where dV denotes a volume element and dV_v is the volume of interconnected pore space which is fully occupied by the mixture of fluid and fluidized particles.
(5) Soil particles are assumed to have been transported and then flown with water or to have remained in the pores, depending on the particle size and flow velocity.
(6) Only those particles that are smaller than the flow-averaged pore size can be transported.
(7) All the particles that are larger than the flow-averaged pore size are deposited in the pores. The soil will stabilize when none of the particles are smaller than the flow-averaged pore size.

In assumptions (6) and (7), the flow-averaged pore size is an important determinant of the particle movement and hence it is further discussed below.

2.1.2. Flow-averaged pore size

Flow cannot be precisely measured at the microscopic pore scale. This study conceptualizes the individual pore as an equivalent of a capillary tube in which flow occurs according to the Hagen–Poiseuille law for capillary flow. If the soil permeability

and the porosity are known, the flow-averaged pore diameter d (m) can be deduced as follows:

$$d^2 = \frac{32K\tau}{\phi} \tag{3}$$

In this expression, K is the soil permeability (m^2) and τ is the tortuosity factor. Salem and Chiligarian [17] reported that the tortuosity factor (τ) responds negatively to porosity (ϕ). The relationship between tortuosity and porosity of a porous medium, with a medium ϕ range, is as follows:

$$\tau = 2.1449 - 0.01126\phi \tag{4}$$

2.1.3. Change in porosity

This study assumed that soil particles simply move with water. Some previous workers have described the relationship between water flow rate and soil particle movement [12–16,18,19]. Additionally, El-Farhan et al. [18] performed four subsequent infiltration experiments. They considered that the curve relating cumulative particle mass collected to cumulative water volume collected is indicative of particle production. The slope of these curves remains relatively constant for individual experiments.

At the start of air sparging in the saturated zone, the injected air displaces the water. The flowing water, which is driven by injected air, causes movement of soil particles in the porous medium. To establish the equation of the increase in porosity, a representative elemental volume (V_e) in the saturated zone is considered. According to the governing equations of this author [15], at the beginning, the injected gas displaces the water in the porous medium and induces particle movement. The volume of injected gas (V_g) equals the sum of the water volume displaced (V_w) and the volume of moved particles (V_p):

$$V_g = V_w + V_p \tag{5}$$

Applying the results of El-Farhan et al. [18], the slope of the curve relating cumulative particle mass collected to cumulative water volume collected remains relatively constant. Hence, the ratio of cumulative mass of moved particles (M_p) and the sum of the water volume displaced (V_w) is assumed to be constant, as follows:

$$\frac{M_p}{V_w} = E \tag{6}$$

where E is a constant. Moreover, the cumulative volume of moved particles is proportional to the cumulative mass of moved particles, as follows:

$$V_p = \frac{M_p}{\rho_p} \tag{7}$$

where ρ_p is the bulk density of the soil particle.

The gas saturation (S_g) in the representative elemental volume with a volume of gas injected is as follows:

$$S_g = \frac{V_g}{V_e} = \frac{V_w + V_p}{V_e} \tag{8}$$

The increase in porosity resulting from particle movement from the representative elemental volume (V_e) is as follows:

$$\Delta\phi = \frac{V_p}{V_e} \tag{9}$$

Substituting Eq. (8) into Eq. (9), the increase in porosity can be written as follows:

$$\Delta\phi = \frac{V_p}{V_w + V_p} S_g \tag{10}$$

Substituting Eqs. (6) and (7) into Eq. (10), the increase in porosity can be expressed as follows:

$$\Delta\phi = CS_g \tag{11}$$

where C equals $E/(\rho_p + E)$.

2.1.4. Correcting the permeability

The increase in porosity changes the soil permeability. Some workers have described the effect of porosity by defining permeability as follows [20]:

$$K = C_s f(\phi) d_e^2 \tag{12}$$

where K denotes the soil permeability (m^2), C_s a constant, $f(\phi)$ a function of the soil porosity, and d_e the mean size of the soil particles (m). The most commonly used form of $f(\phi)$ is as shown in Eq. (13):

$$f(\phi) = \frac{\phi^3}{(1-\phi)^2} \tag{13}$$

The constant C_s used in this study is 3.05×10^{-3} [21].

2.2. Physical system

To simplify the numerical simulation, a hypothetical physical system was used in the present case study. The hypothetical system considered here is a 10-m-deep sandy aquifer, bounded on the bottom by an impervious barrier. The groundwater surface lies 4.8 m below the ground surface, and the saturated zone is 5.2 m deep. Additionally, there is a capillary fringe of 0.5 m. The soil simulated in this system is a sand–silt mixture with a density of 2.55 g/cm^3, soil porosity of 0.27 and reservoir permeability of 1.95×10^{-12} m^2. The particle-size distribution of the "initial soil" used in this work is shown in the form of the curve of "$\phi = 0.27$" in Fig. 1. Fig. 2 shows the cross-section and locations of the sparging well and the soil vapor extraction well. The screen of the sparging well was installed 8.4–9.3 m below the ground level and that of the soil vapor extraction well 2.4–3.9 m below.

2.3. Numerical simulator for air sparging

The model, developed by Young [22,23], of a multicomponent multiphase flow in a porous medium was used to simulate the distribution of gas saturation for air sparging [16,24]. The target site had to be segmented into several grids before simulation. The model inputs required were flow rates, pressures, and the characteristics of groundwater and soil,

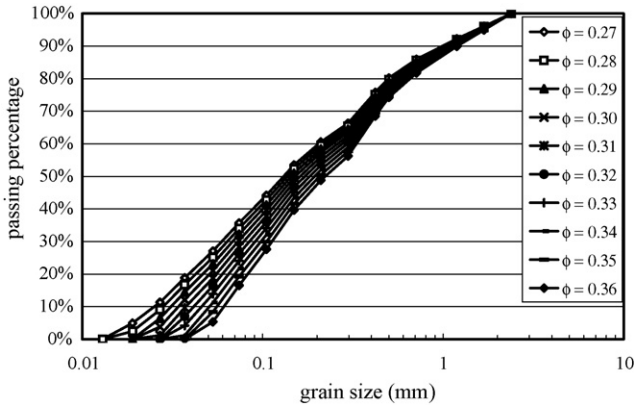

Fig. 1. Particle-size distribution for soils of different porosities.

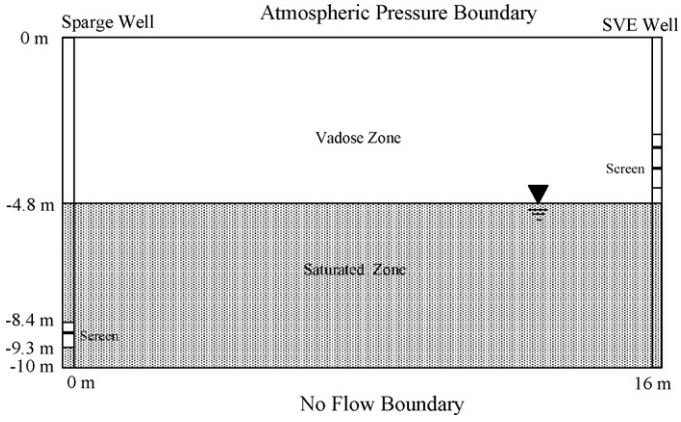

Fig. 2. Cross-sections and locations of the sparging well and soil vapor extraction well.

such as porosity, intrinsic permeability, relative permeability and capillary pressure (Table 1). Fig. 3 shows the simulated gas saturation profile of the aquifer before revising the air sparging simulation parameters.

2.4. Source of value C

C equals $E/(\rho_p + E)$. ρ_p is the bulk density of the soil particle and is a constant. E is the ratio of cumulative mass of moved particles (M_p) and the sum of the water volume displaced (V_w) [16]. E depends on the forcing of air sparging, and on the properties of fluid and soil. For example, soil particles are either transported with water or remain in the pores, depending on the particle size and flow velocity. Only those particles that are smaller than the flow-averaged pore size can be transported. E may be regarded as a constant for a remediation site and for a controlled air sparging process. Hence, C is also a constant in a case study.

Table 1
Parameters for air sparging simulations

Parameters	Before revision
Porosity	0.27
Permeability (m^2)	1.95×10^{-12}
Residual water saturation	0.15
Well diameter (cm)	5
Injected pressure (kPa)	27.5
Air flow rate (m^3/min)	0.46
Reservoir temperature (°C)	20
n (relative permeability functions)[a]	3
α_{gw}[a]	5.2
S_m[a]	0.0
n (capillary pressure functions)[a]	1.84

[a] From McCray and Falta [3] for sandy medium. α_{gw} and S_m are empirically determined and are assumed to be constants of the porous medium.

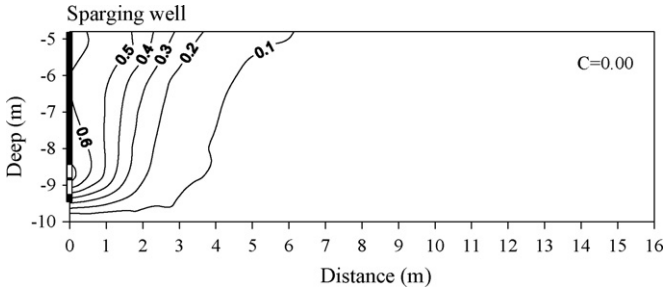

Fig. 3. Simulated gas saturation profile before parameter revision.

The author's previous works [15,16] indicated that the average increase in porosity is about 0.04 for both laboratory and field tests. According to the linear function of Eq. (11), this study estimates that the maximum increase in porosity is 0.09 for all simulation grids by comparing the average and maximum gas saturation (0.33 and 0.75, respectively) around the injection well in Fig. 3. From Eq. (11), the corresponding C is 0.12 for the given maximum increase in porosity. This study discussed the influences in ROI and swept volume when $C = 0.12$. Moreover, the other constant C, $C = 0.02$, 0.04, 0.06, 0.08, 0.10, which are smaller than 0.12, were also used in this study to understand the variation in the increase in constant C.

3. Results and discussion

3.1. Effect of particle movement on particle-size distribution and porosity change

This study assumes that only those particles that are smaller than the flow-averaged pore size can be transported. Therefore, it is important to compare the particle size and flow-averaged pore size. Fig. 1 shows the particle-size distributions of soil for porosities of 0.27–0.36 and Table 2 lists the particle size and flow-averaged pore size for soils of different porosities. For porosity of 0.27, D_{50} (50% particle size) and D_{80} (80% particle size) values are 0.132 mm and 0.497 mm and for porosity of 0.36, these values are 0.224 mm and 0.661 mm, respectively, and they are almost proportional to the porosity. The minimum soil particle size was smaller than the flow-averaged pore size and therefore, some small particles could be transported freely in the soil.

3.2. Relationships among gas saturation, porosity and permeability

Using Eq. (11) and constant C, where $C = 0.02$, 0.04, 0.06, 0.08, 0.10 and 0.12, the relationships between the increase in

Table 2
Change in grain and pore sizes for different porosities

Porosity	D_{50} (mm)	D_{80} (mm)	D_{min} (mm)	Flow-averaged pore diameter (mm)
0.27	0.132	0.497	0.013–0.019	0.021
0.28	0.138	0.512	0.013–0.019	0.023
0.29	0.145	0.530	0.019–0.027	0.025
0.30	0.151	0.549	0.019–0.027	0.027
0.31	0.157	0.568	0.019–0.027	0.030
0.32	0.163	0.586	0.027–0.037	0.033
0.33	0.169	0.605	0.027–0.037	0.035
0.34	0.196	0.623	0.027–0.037	0.043
0.35	0.207	0.642	0.037–0.053	0.047
0.36	0.224	0.661	0.037–0.053	0.054

porosity and gas saturation are shown in Fig. 4. Each straight line in the figure corresponds to a constant C value. For this case study, following Eqs. (12) and (13), the relationship between permeability and porosity is shown in Fig. 5. The maximum change in porosity occurred near the screen of the sparging well. Table 3 lists the maximum change in porosity and permeability for different values of constant C. The maximum porosity changed from 0.27 to 0.30, 0.33 and 0.36 given $C = 0.04$, 0.08 and 0.12; the maximum permeability changed from 1.95×10^{-12} m^2 to 3.77×10^{-12} m^2, 6.88×10^{-12} m^2 and 1.73×10^{-11} m^2. When constant C reached 0.12, the maximum change in porosity was 0.09 and intrinsic porosity 0.36 (upper limit of porosity).

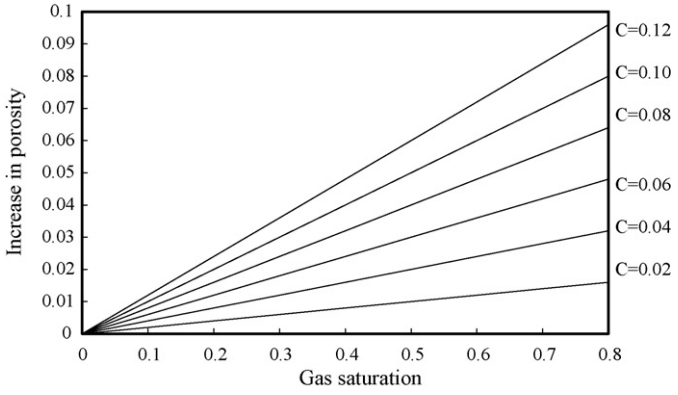

Fig. 4. Relationship between the increase in porosity and gas saturation.

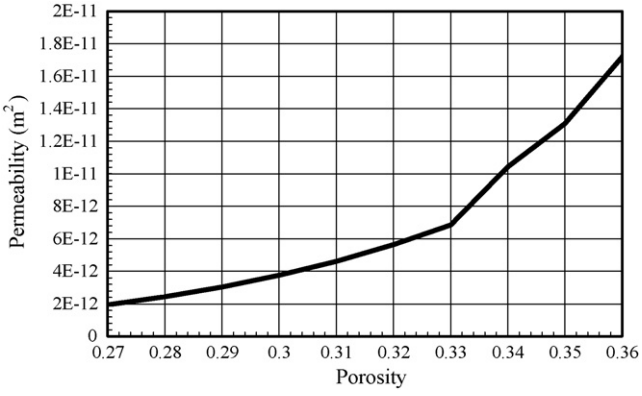

Fig. 5. Relationship between the porosity and permeability.

3.3. Change in gas saturation profile

After correcting the porosity and permeability according to constant C, and re-running the simulator, gas saturation profiles were obtained for $C = 0.02$, 0.04, 0.06, 0.08, 0.10 and 0.12, as shown in Fig. 6. The contours of gas saturation get closer to the sparging well with increasing constant C, regardless of whether the contour was 0.1, 0.2, 0.3, 0.4 or 0.5. This phenomenon occurred because parts of the soil particles were transported. Consequently, permeability of the soil near the sparging well increases and so does the gas flow to this zone, relative to other zones. Therefore, the gas flow lines are concentrated in the zone where the permeability is relatively high. In this study, ROI was estimated from Figs. 3 and 6 on the assumption that it is the distance from the sparging well to where the gas saturation is 0.1. From the figures it can be seen that the ROIs at a depth of 9 m are approximately 3.3 m and 2.5 m before ($C = 0.00$) and after ($C = 0.12$) the revision of the porosity and permeability. If the ROI is assumed to be the distance from the sparging well to where the gas saturation is 0.2, the ROIs at 9 m depth are approximately 2.0 m and 1.3 m before ($C = 0.00$) and after ($C = 0.12$) the revision of the porosity and permeability.

3.4. Change in swept volume of air sparging

Based on the model output data, the distribution of gas saturation around the sparging well is shown in Fig. 6 after correction values of $C = 0.02$, 0.04, 0.06, 0.08, 0.10 and 0.12 were used in the simulation. Fig. 3 shows that the gas flowed through a larger area than was indicated by Fig. 6. For $C = 0.00$, the swept volume

Table 3
Maximum change in porosity and permeability for different constant C_s

Constant C	Maximum change in porosity	Maximum change in permeability (m^2)
0.02	0.015	8.00×10^{-13}
0.04	0.030	1.82×10^{-12}
0.06	0.045	3.20×10^{-12}
0.08	0.060	4.93×10^{-12}
0.10	0.075	9.91×10^{-12}
0.12	0.090	1.53×10^{-11}

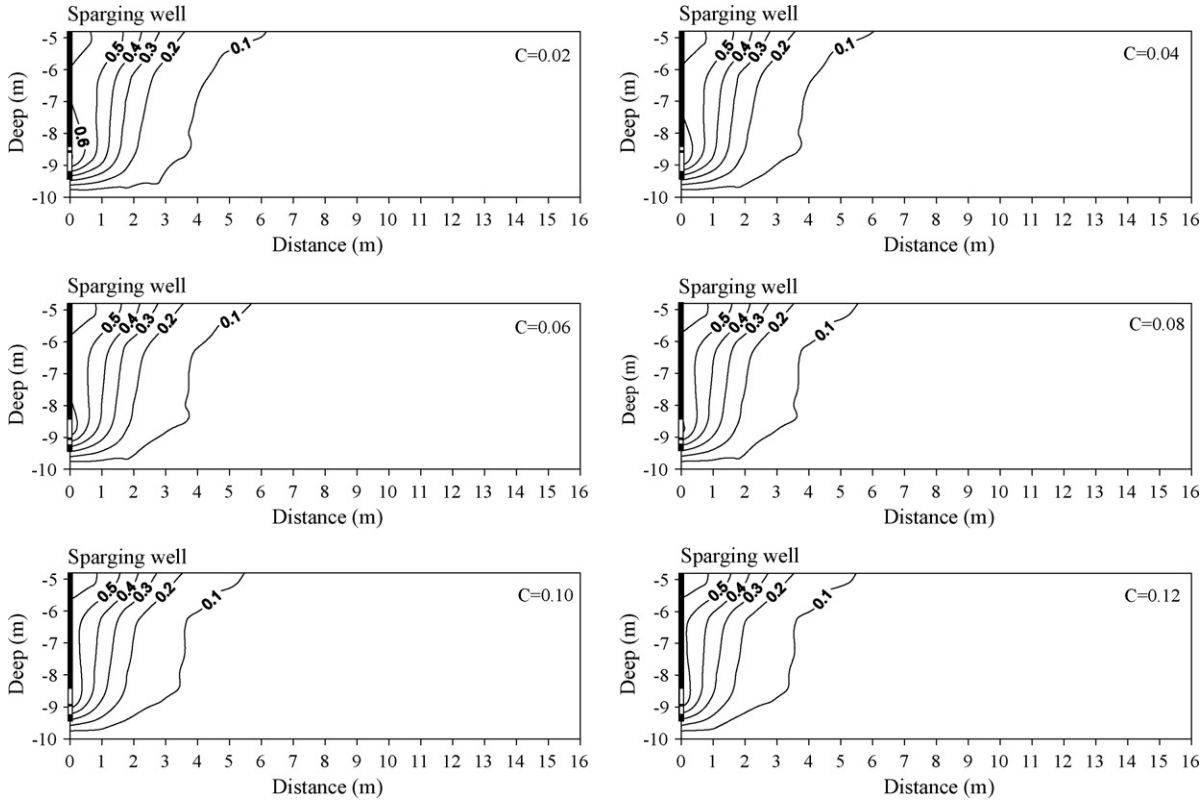

Fig. 6. Simulated gas saturation profiles after the porosity and permeability were revised for $C = 0.02$, 0.04, 0.06, 0.08, 0.10 and 0.12.

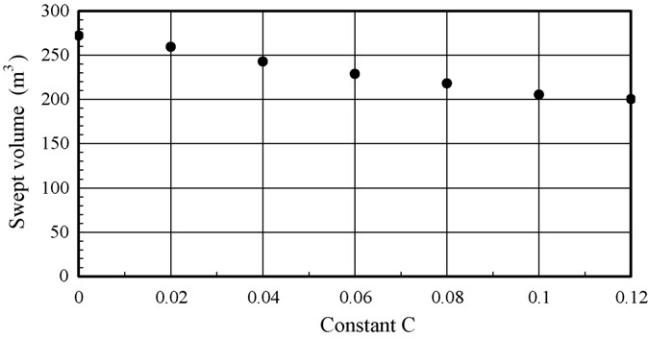

Fig. 7. Relationship between the constant C and swept volume.

was estimated to be 272 m^3 for the zone where the gas saturation exceeded 10%. For $C = 0.02$, 0.04, 0.06, 0.08, 0.10 and 0.12, the swept volumes were changed from 272 m^3 to 250 m^3, 243 m^3, 229 m^3, 218 m^3, 205 m^3, and 200 m^3. Fig. 7 shows the relationship between the constant C and the swept volumes. This study demonstrates that the remediated zone was obviously reduced in size when soil particles were transported during air sparging.

4. Conclusions

This study developed a method for estimating the changes in ROI and swept volume during air sparging by combining the concepts of particle internal stability, and the relationships between flow rate and particle movement and between porosity and permeability. From the methods developed, the following observations are made:

- During air sparging, some soil particles are transported around the sparging well. Consequently, the permeability of the soil near the sparging well increased and so did the gas flow to this zone, relative to other zones. Therefore, gas flow lines were concentrated in the zone where the permeability was relatively high. In addition, ROI is expected to decrease if soil particles are transported.
- The swept volume clearly decreases when soil particles are transported during air sparging. In this case study, the swept volume of the sparging well at $C = 0.12$ is significantly reduced, and becomes 73% of the swept volume at $C = 0.00$.

This study demonstrates a method of evaluating the remediated zone in which the soil particles are transported during air sparging. As constant C is the most important determinant in this method, some experimental and theoretical work, such as slug test or field tracer test [14], has to be carried out to estimate its value before performing air sparging at real-world contamination sites.

Acknowledgements

The author would like to thank the National Science Council of the Republic of China, Taiwan for financially supporting this research under Contract No. NSC 90-2218-E-434-001.

References

[1] W. Braida, S.K. Ong, Air sparging effectiveness: laboratory characterization of air-channel mass transfer zone for VOC volatilization, J. Hazard. Mater. B 87 (2001) 241–258.

[2] W. Ji, A. Dahmani, D.P. Ahlfeld, J.D. Lin, E.H. Hill III, Laboratory study of air sparging: air flow visualization, Ground Water Monit. Rem. 13 (1993) 115–126.

[3] J.E. McCray, R.W. Falta, Defining the air sparging radius of influence for groundwater remediation, J. Contam. Hydrol. 24 (1996) 99–110.

[4] J.E. McCray, R.W. Falta, Numerical simulation of air sparging for remediation of NAPL contamination, Ground Water 35 (1997) 99–110.

[5] K.R. Reddy, J.A. Adams, Effects of soil heterogeneity on air flow patterns and hydrocarbon removal during in-situ air sparging, J. Geotech. Geoenviron. 127 (2001) 234–247.

[6] F.J. Santarelli, Sand production on water injectors: Just how bad can it get, Paper SPE 47329 presented at the SPE/ISRM Eurock'98 held in Trondheim, Norway, July 8–10, 1998.

[7] E. Papamichos, I. Vardoulakis, J. Tronvoll, A. Skjvrstein, Volumetric sand production model and experiment, Int. J. Numer. Anal. Met. 25 (2001) 789–808.

[8] J. Moghadasi, H. Muller-Steinhagen, M. Jamialahmadi, A. Sharif, Theoretical and experimental study of particle movement and deposition in porous media during water injection, J. Petrol. Sci. Eng. 43 (2004) 163–181.

[9] M.E. O'Neill, A sphere in contact with a plane wall in a slow linear shear flow, Chem. Eng. Sci. 23 (1968) 1293–1298.

[10] G.A. Gillespie, Effective monitoring screen for fine sand aquifers, ASTM Special Techn. Publ. 1118 (1992) 241–255.

[11] Y. Zevi, A. Dathe, B. Gao, B.K. Richards, T.S. Steenhuis, Quantifying colloid retention in partially saturated porous media, Water Resour. Res. 42 (2006) W12S03.1–W12S03.13.

[12] D.I. Kaplan, P.M. Bertsch, D.C. Adriano, W.P. Miller, Soil-borne mobile colloids as influenced by water flow and organic carbon, Environ. Sci. Technol. 27 (1993) 1193–1200.

[13] D.I. Kaplan, M.E. Summer, P.M. Bertsch, D.C. Adriano, Mineralogical and physicochemical differences between mobile and nonmobile colloidal phases in reconstructed pedons, Soil Sci. Soc. Am. J. 61 (1997) 641–649.

[14] L.N. Reddi, R.S. Govindaraju, Particle mobilization in sand-clay mixtures and facilitation of contaminant removal—critical shear stress concept, Geotech. Special Publ. 46 (1995) 1222–1236.

[15] Y.J. Tsai, D.F. Lin, Mobilizing particles in a saturated zone during air sparging, Environ. Sci. Technol. 38 (2004) 643–649.

[16] Y.J. Tsai, Soil-particle movement and porosity/permeability change during in situ air sparging, J. Hazard. Mater. 142 (2007) 315–323.

[17] H.S. Salem, G.V. Chilingarian, Influence of porosity and direction of flow on tortuosity in unconsolidated porous media, Energy Sources 22 (2000) 207–213.

[18] Y.H. El-Farhan, N.M. Denovio, J.S. Herman, G.M. Hornberger, Mobilization and transport of soil particles during infiltration experiments in an agricultural field, Shenandoah Valley, Virginia, Environ. Sci. Technol. 34 (2000) 3555–3559.

[19] N. Weisbrod, O. Dahan, E.M. Adar, Particle transport in unsaturated fractured chalk under arid conditions, J. Contam. Hydrol. 56 (2002) 117–136.

[20] B.B. Rajani, A simple model for describing variation of permeability with porosity for unconsolidated sands, In Situ 12 (1988) 209–226.

[21] M. Locke, B. Indraratna, G. Adikari, Time-dependent particle transport through granular filters, J. Geotech. Geoenviron. 127 (2001) 521–529.

[22] L.C. Young, R.E. Stephenson, A generalized compositional approach for reservoir simulation, Soc. Petrol. Eng. J. (1983) 727–742.

[23] L.C. Young, Full-field compositional modeling on vector processors, SPE Reservoir Eng. (1991) 107–114.

[24] Y.J. Tsai, M.C.T. Kuo, T.S.E. Huang, Air sparging tracer test to investigate the flow path, J. Environ. Sci. Health Part A 36 (2001) 999–1014.